S.T. Yau High School Science Award

Research Report

The Team

Name of team member: Ruojin Zhang

School: Northview High School

City, Country: Johns Creek, GA, United States

Name of supervising teacher: Azmathunnissa Azeem

Job Title: Chemistry Teacher

School/Institution: Northview High School

City, Country: Johns Creek, GA, United States

Title of Research Report

Nature's Blueprint: Data-Driven Design of Feather Microstructures for Enhanced Surface Water Repellency

Date

September 15th, 2026

Nature's Blueprint: Data-Driven Design of Feather Microstructures for Enhanced Surface Water Repellency

Abstract

Water-repellent coatings across aviation, construction, and textiles still rely overwhelmingly on per- and polyfluoroalkyl substances (PFAS), which are persistent chemicals with environmental half-lives exceeding 50 years that bioaccumulate through food chains. Removing PFAS contamination at current emission rates would exceed the global GDP of roughly US$106 trillion, yet high-performance substitutes remain scarce. Avian feathers offer a different strategy: they maintain hydrophobicity through hierarchical microstructures rather than surface chemistry, while remaining flexible and resilient. Prior quantitative work has characterized feather wettability almost entirely through barbule spacing, diameter, or density. Yet, the role of barbule angle, particularly the asymmetry between distal and proximal angles, has never been quantified as a predictor despite its apparent contribution to forming a feather's mesh-like structure. Critically, no prior work validates the role of this novel parameter by combining multivariable modeling with physical fabrication. This study investigates whether feather-derived microgeometric rules can be quantified, computationally modeled, and translated into fabricated surfaces with enhanced water repellency. We established a closed-loop biomimetic framework linking biological measurement, machine-learning analysis, and 3D-printed validation. Molted flight and contour feathers from 12 species spanning nine avian orders and both aquatic and terrestrial habitats were imaged via scanning electron microscopy to extract seven barbule parameters, each paired with sessile-drop contact angle measurements and evaluated using linear, generalized additive, and machine learning models. Nonlinear models outperformed linear models: Random Forest achieved a cross-validated R^2=0.509 for the full dataset and R^2=0.833 for terrestrial contour feathers. At the species level, the difference between proximal and distal angles was the dominant structural correlate of contact angle, with highly asymmetric feathers averaging 8.8° more than low-asymmetric feathers. To physically validate our machine learning classifications, we fabricated feather-inspired surfaces matching predicted high, biological-reference, and low performance groups, yielding contact angles of 90.7°, 85.0°, and 62.3°, respectively, against a flat control of 72.0°, perfectly mirroring asymmetric and machine learning trends. The high-performance design crossed the 90° hydrophobic threshold on an intrinsically hydrophilic resin, increasing contact angle by 18.7° (25.97%) over the flat control. Although within-species variation and sampling size restrict immediate cross-species predictability, our results conclusively demonstrate that structural asymmetry and optimized microstructures offer a novel, chemistry-free pathway to water repellency.

Keywords: Biomimicry, Hydrophobicity, Machine Learning, Feather-Inspired Materials, Feather Morphology, Contact Angle

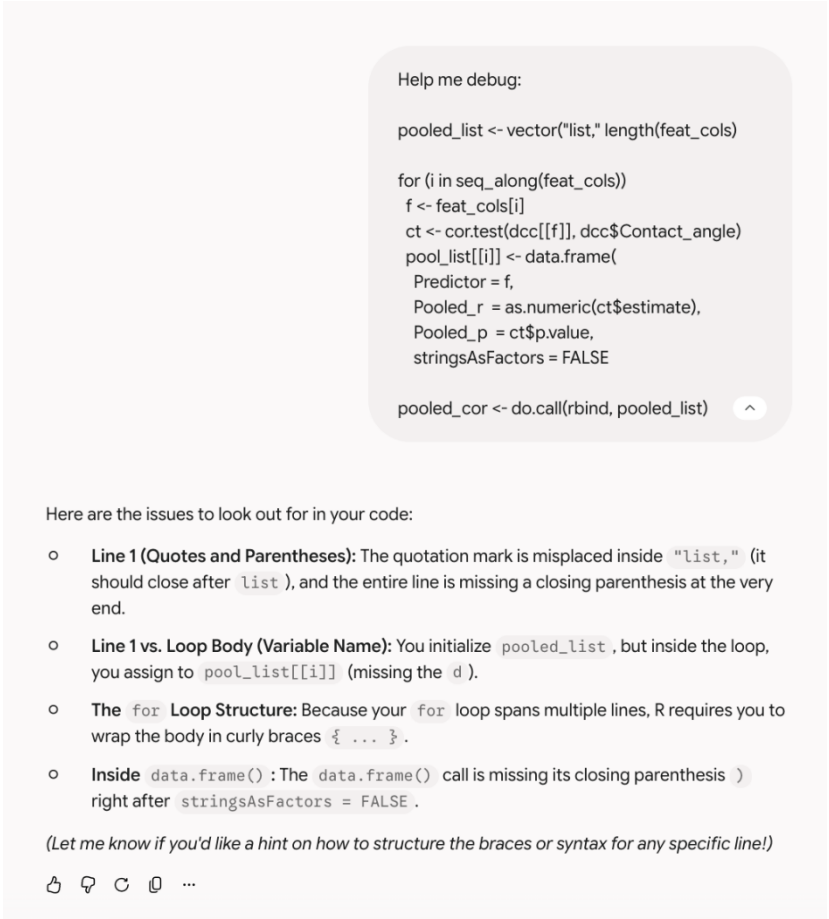
Acknowledgments

This research was driven by a deep fascination with birds, specifically the microstructural properties of feathers that optimize both water repellency and aerodynamic efficiency. After traveling across 5 continents and viewing more than 600 species globally, I began this independent project from start to finish. I am immensely grateful to the Cornell Lab of Ornithology for providing vital inspiration for species sampling. Special thanks are extended to the Shanghai Zoo and its husbandry staff for granting permission to collect fallen feathers during the molting season. I sincerely appreciate Professor Liu and the faculty at Donghua University for their invaluable supervision and for providing me access to essential experimental and fabrication equipment.

I am equally grateful to Professor Richard Prum (Yale University) for his critical insights during the fabrication phase; Jordan (Cornell Lab of Ornithology) for assistance in identifying potential methodological biases during our consultations; Zsófia Szegletes (University of California, Santa Barbara) for guidance in research development; and the faculty at the Smithsonian feather collection for their logistical support. Additionally, I would like to thank Ms. Azmathunnissa Azeem at Northview High School for her insightful guidance regarding the potential confounding effects of uropygial oil during the feather cleaning process. Finally, the collective support from these institutions and individuals beautifully highlights the interconnected and collaborative nature of the global scientific community.

AI Usage Statement

All content and analysis code was written independently by me. Gemini and Grammarly were used as AI tools as a supplement to this work, specifically including Gemini for debugging and troubleshooting code errors, and Grammarly for checking grammar and basic punctuation. No AI was involved in the active creation of new content and interpretation of results. All tasks done by AI involve human oversight and are initiated by authors to resolve code errors, and no sensitive information is shared. All decisions are based on my independent judgments.



Help me debug:

```
pooled_list <- vector("list," length(feat_cols)

for (i in seq_along(feat_cols))
 f <- feat_cols[i]
 ct <- cor.test(dcc[[f]], dcc$Contact_angle)
 pool_list[[i]] <- data.frame(
  Predictor = f,
  Pooled_r  = as.numeric(ct$estimate),
  Pooled_p  = ct$p.value,
  stringsAsFactors = FALSE

pooled_cor <- do.call(rbind, pooled_list)
```

Here are the issues to look out for in your code:

- **Line 1 (Quotes and Parentheses):** The quotation mark is misplaced inside `"list,"` (it should close after `list`), and the entire line is missing a closing parenthesis at the very end.
- **Line 1 vs. Loop Body (Variable Name):** You initialize `pooled_list`, but inside the loop, you assign to `pool_list[[i]]` (missing the `d`).
- **The `for` Loop Structure:** Because your `for` loop spans multiple lines, R requires you to wrap the body in curly braces `{ ... }`.
- **Inside `data.frame()`:** The `data.frame()` call is missing its closing parenthesis `)` right after `stringsAsFactors = FALSE`.

(Let me know if you'd like a hint on how to structure the braces or syntax for any specific line!)

Declaration of Academic Integrity

The participating team declares that the paper submitted is comprised of original research and results obtained under the guidance of the instructor. To the team's best knowledge, the paper does not contain research results, published or not, from a person who is not a team member, except for the content listed in the references and the acknowledgment. If there is any misinformation, we are willing to take all the related responsibilities.

Names of team members Ruojin Zhang

Signatures of team members

Name of the instructor Azmathunnissa Azeem

Signature of the instructor

Date Sept 4, 2026

Contents

1. Introduction 1

2. Methodology 3

2.1. Study Design and Sampling Strategy 3

2.2. Microstructural Characterizations and Parameter Definitions 5

2.3. Contact Angle Measurement 6

2.4. Computational Analysis and Statistical Methods 7

3. Results and Analysis 8

3.1. Cross-Species Overview: Contact Angle Differs Significantly Across Species 8

3.2. Mechanistic Drivers in Pooled and Cross-Species Data: Asymmetry Influences Hydrophobicity 9

3.3. Computational Modeling: Structure Predicts Hydrophobicity in Non-Linear Models 10

3.4. Stratification Analysis: Structure Predicts Best in Terrestrial Contour Feathers 11

3.5. Generalization and Variance Structure: Models Cannot Extrapolate Across Species 13

3.6. Verification Through 3D Fabrication of Feather Microstructures Confirms Model Robustness 14

4. Discussion 16

4.1. Mechanistic Explanations and Habitat-Dependent Strategies 16

4.2. Interpretation of Fabrication Results 17

4.3. Limitations 18

4.4. Implications 18

4.5. Applications 19

4.6. Future Work 19

5. Conclusion 20

References 21

1. Introduction

Engineered water-repellent surfaces are essential across industries such as anti-icing for aerospace [1], self-cleaning in infrastructure [2], biomedical devices [3], and textiles [4], but most rely on fluorinated polymers or silicone treatments [5]. The fluorinated coatings belong to the PFAS class of forever chemicals under close attention of the European Union and the United States, with environmental half-lives beyond 50 years [6]. Between 20,000 and 100,000 metric tonnes are released each year, and removing this pollution would cost more than the entire global GDP of roughly US$106 trillion [7]. Therefore, durable and low-impact alternatives to chemical coatings have become a necessary step toward an efficient and green future.

Biomimicry offers a promising path for obtaining structural hydrophobicity without such harmful coatings. Among nature-inspired examples are the lotus leaf [8] and cicada wings [9], which trap air with their microarchitecture to minimize solid-liquid contact. Although progress in superhydrophobicity has been achieved on these biological systems, they are limited in their rigidity and lack variation for engineers to derive optimized designs.

In contrast, avian feathers achieve persistent hydrophobicity through hierarchical structure while remaining flexible, porous, and resilient across motion and repeated wetting. Additionally, birds have evolved over evolutionary time, offering individual variations between species and feather types that engineers can leverage. Therefore, they constitute a transferable design with huge potential that remains currently underexplored.

Currently, structural hydrophobicity is understood by the measurement of contact angle (CA), which is the angle at the solid-liquid-air boundary, with higher angles indicating stronger surface hydrophobicity. The fundamental framework guiding it is the Cassie-Baxter regime, where droplets rest on trapped air pockets on rough, microstructured surfaces, thereby minimizing their solid-liquid contact [10]. This regime is specifically apparent in birds, where feather hydrophobicity arises from their structure instead of surface chemistry or their keratin composition, which is itself hydrophilic [11]. Although existing work has questioned whether factors such as the naturally secreted uropygial oil may affect hydrophobicity, recent work has confirmed its role as merely aiding maintenance rather than providing primary waterproofing; the main driver is still the geometry itself [12].

The quantification of microstructures has therefore become an area of investigation. Rijke (1968) initially used the structural index ((R+D) / R) to relate barb diameter and spacing as a

predictor of structural repellency [13]; however, this index has been largely refuted, since reducing a feather's complexity to a single index is counterproductive [14], [12]. Modern quantitative approaches mainly focus on spacing of barbules, diameter, or density, and their relationships with habitat and hydrophobicity. For example, Srinivasan et al. (2014) quantified a dimensionless barbule spacing ratio (D*) [15], and Pap et al. (2015, 2017) used barb and barbule density correlated with habitat [16], [17]. Muzio et al. (2026) also focused on barbule density via micro-CT-based 3D modeling to reveal how higher barbule density reduces water repellency [18].

Although robust work has been established to explain this dynamic, effects of new parameters, multivariable approaches, or closed-loop fabrication remain largely unexplored. Barbule angle, and especially the asymmetry of a feather vane between a barb to barbule, has never been quantified as a true predictor. The distinction between distal and proximal barbules has been historically recorded, with distal barbules being shorter and more spinous [19], [20], but such accounts remain highly qualitative, with no numeric link to wettability. Therefore, understanding the angular composition may lead to new insights on how intersections form the anisotropic mesh of the whole feather design. Additionally, most parameter-and-function work treats predictors in isolation, which contrasts with the interactive nature of feathers where all parameters contribute to the overall hierarchy. Machine learning excels at multivariable analysis, but has only been applied to predict contact angle on synthetic and engineered surfaces [21]. Existing literature rarely applied multivariable modeling to biological feather microstructures across diverse scopes, such as phylogeny and habitat. Lastly, limited research closes the loop from measurement to fabrication. While feather-inspired surfaces have been fabricated [22], few, if any, derive a specific predictor from biological data and then fabricate structures to validate it.

In this study, we hope to address these gaps by offering a proven example where biological data informs model predictions, which are in turn validated by external fabrication of model-optimized surfaces. To do so, we conducted a cross-species multivariable investigation of feather microstructure and hydrophobicity. We aimed to quantify microstructures and identify which parameter governs wettability principles using multivariable machine learning. To understand the extent to which these predictions hold, we tested their ability to be generalized across species and validated the dominant predictor physically by fabricating and testing feather-inspired 3D microstructures. Results from printed structures establish whether chemistry-free, structurally driven design principles can be extracted from biology and engineered into sustainable water-repellent surfaces.

2. Methodology

2.1. Study Design and Sampling Strategy

We conducted a cross-species, multi-feather comparative study pairing quantified barbule geometry with static contact angle (CA) as a measurement of surface hydrophobicity (**Fig. 1**). We chose 12 representative species from nine major avian orders (spanning from basal lineages in order Struthioniformes to recently diverged Passeriformes) and ecological diversity (Aquatic/semi-aquatic to terrestrial) to maximize phylogenetic breadth and test structural relationships beyond a single lineage (**Table. 1**). Relative phylogeny estimates are based on Cornell Lab of Ornithology Birds of the World Phylogeny Explorer (**Fig. 2A**).

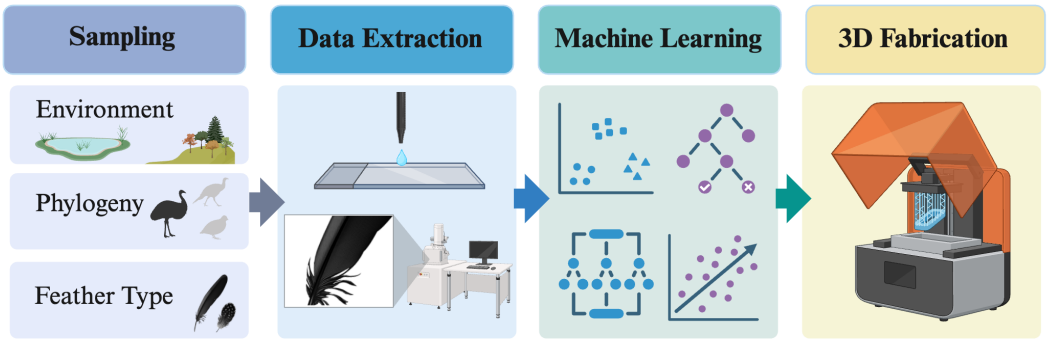


Figure 1. Overview of the cross-species workflow. Molted flight and contour feathers from 12 species spanning the avian phylogeny were imaged by scanning electron microscopy to quantify barbule microgeometry and measured by static contact angle (CA). Paired structural and wetting data were analyzed with multivariable machine learning, and the dominant predictor was validated through biomimetic 3D fabrication. Created with BioRender.

Aquatic species are defined as species that are considered waterfowl and wading birds who spends a majority of their lives in proximity to water. In this study, we sourced 5 aquatic-associated species to determine habitat-related trends, ranked by their relative time of divergence, including Anas poecilorhyncha (Spot-billed duck), Cygnus olor (Mute swan), Phoenicopterus roseus (Greater flamingo), Eudocimus ruber (Scarlet ibis), and Pelecanus onocrotalus (Great white pelican).

The seven terrestrial species are defined as species evolved to live and reproduce primarily on land. Ranked by relative divergence, they include: Struthio camelus (Ostrich), Phasianus colchicus (Common pheasant), Bubo bubo (Eurasian eagle-owl), Dendrocopos major (Great spotted woodpecker), Psittacula eupatria (Alexandrine parakeet), Pica pica (Eurasian magpie), and Passer domesticus (House sparrow).

Table 1. Selected Species for Study and Habitat Classification

Common Name	Scientific Name	Habitat Classification
Ostrich	Struthio camelus	Terrestrial
Spot-billed duck	Anas poecilorhyncha	Aquatic
Mute swan	Cygnus olor	Aquatic
Common pheasant	Phasianus colchicus	Terrestrial
Greater flamingo	Phoenicopterus roseus	Aquatic
Scarlet ibis	Eudocimus ruber	Aquatic
Great white pelican	Pelecanus onocrotalus	Aquatic
Eurasian eagle-owl	Bubo bubo	Terrestrial
Great spotted woodpecker	Dendrocopos major	Terrestrial
Alexandrine parakeet	Psittacula eupatria	Terrestrial
Eurasian magpie	Pica pica	Terrestrial
House sparrow	Passer domesticus	Terrestrial

Evolutionary and ecological characteristics of the 12 sampled species, including scientific name, common name referenced throughout this report, and classified habitat. Species are presented in order of relative divergence, spanning from basal palaeognaths to recently diverged passerines.

To investigate whether various functional demands, such as aerodynamics compared to insulation/waterproofing, we sourced 6 flight and contour feathers, except for the House sparrow and Scarlet Ibis, where only flight feathers were collected due to collection constraints. Because these feather types experience different mechanical and environmental demands, analyzing both provides insight into functional trade-offs in microstructural design. All feathers are sourced ethically (collection of natural fall-offs during molting season) in collaboration with the Shanghai Zoo to ensure the safety of birds (**Fig. 2B**). To ensure safety and remove confounding uropygial oils atop the feather surface, all samples are rinsed twice with hexane and deionized water solution, then dried overnight. Previous literature has demonstrated that such procedures do not dramatically alter microstructures [23].

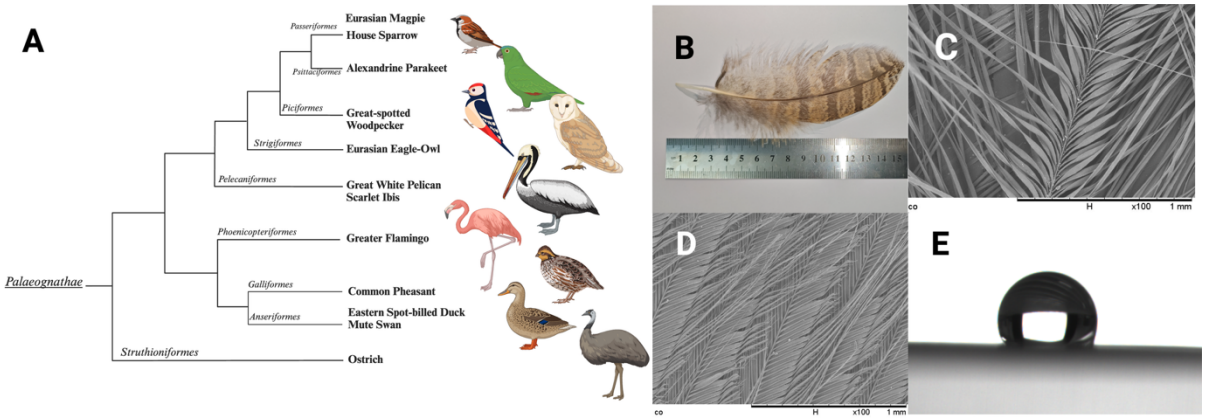


Figure 2. Study design and structural diversity of sampled species. (A) Relative phylogenetic divergence of the 12 species. Created with BioRender. (B) Sample feather demonstrating the standard for collection from a zoo. (C) Representative flight feather SEM image of the ostrich. (D) Representative SEM image of a contour feather of the Eurasian eagle-owl. (E) Sample CA without a device measurement label, demonstrating hydrophobicity on the top of the feather surface.

2.2. Microstructural Characterizations and Parameter Definitions

Scanning electron microscopy (SEM) was employed to visualize feather microstructure prior to ImageJ processing to extract quantitative geometric parameters (**Fig. 2C-D**). We first sputter-coated feather samples with an approximately 10 nm layer of gold to render the non-conductive keratin surface electrically conductive and to prevent charging artifacts. Imaging was performed using a TM3000 SEM at a working distance of 9800 µm, an emission current of 55200 nA, and a filament current of 1850 mA.

Parameter extraction from SEM imaging is divided into length, angle, and spacing (**Fig. 3**). To investigate the effect of the length in relation to CA, we first recorded the basal lamella (or ribbon-like proximal region) length of a barbule in µm, or L_{basal}. We also measured the total length of a barbule, L_{total}, as well as the basal length ratio, R_{basal}, as shown in Equation (1).

$$R_{basal} = \frac{L_{basal}}{L_{total}} \tag{1}$$

Barbule spacing, or $d_{barbule}$, represents the mean center-to-center distance between adjacent barbules in µm (**Fig. 3**). Angle relationships between the barb and barbule are also measured to examine anisotropy and contributions to the mesh-like coverage (**Fig. 3**). The angle between the barb rachis and the distal barbules (upper side, pointing toward the feather's

tip) is the distal angle, or θ_{distal}, measured in degrees, while the angle between the barb rachis and the proximal barbules is expressed as proximal angle, or θ_{proximal}. The barbule angle asymmetry, expressed as an absolute difference between the distal and proximal angles, is defined as Δθ, described in equation (2).

$$\Delta\theta = \left|\theta_{\text{distal}} - \theta_{\text{proximal}}\right| \tag{2}$$

25 measurements are averaged per parameter per image to reduce operator and tracing error in ImageJ. This ensures our per-sample values are stable. Four images from flight feathers and two from contour feathers, taken from different spatial locations, were analyzed per species. This approach yielded over 8,000 individual data points in total, with mean values from each 25-point set paired directly with corresponding CA measurements.

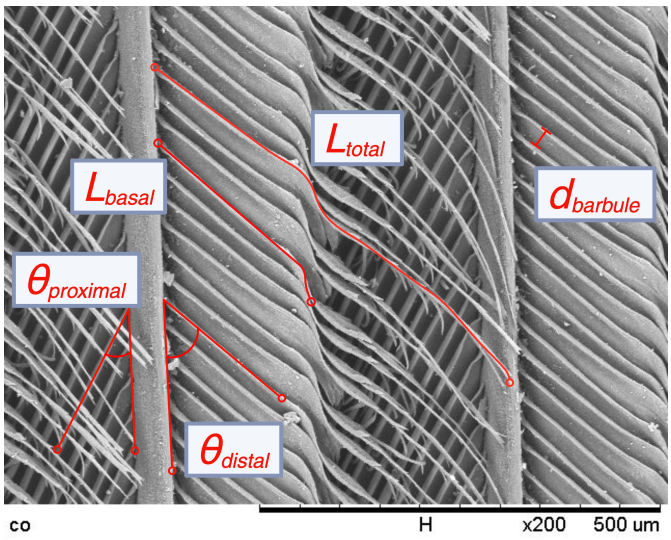


Figure 3. Barbule parameters measured on a representative scanning electron micrograph. The distal barbule angle (θ_{distal}) and proximal barbule angle (θ_{proximal}) are measured between the barb and the distal and proximal barbules. The angle asymmetry ($\Delta\theta$) is their absolute difference. Basal section length (L_{basal}), total barbule length (L_{total}), and barbule spacing (d_{barbule}) are indicated. Twenty-five measurements per parameter were averaged per image.

2.3. Contact Angle Measurement

The sessile drop method was used in a contact angle goniometer (Dataphysics OCA20) with a droplet volume of 5 µL for each of 12 measurements per species (**Fig. 2E**). Placement locations are aligned with subsequent SEM imaging sites to directly pair the structure with its hydrophobic performance. The apparent contact angle reflects the trapped-air/solid-fraction

geometry, so CA serves as an integrative readout of microstructure rather than surface chemistry, described in the Cassie–Baxter equation (3), where θ_{CB} is the apparent CA in the Cassie-Baxter state [10], θ_Y is the intrinsic CA of the keratin/resin per Young's equation [24], and f_s is the solid fraction in contact with the droplet.

$$cos\ \theta_{CB} = f_s\ (cos\ \theta_Y + 1) - 1 \tag{3}$$

Because feather surfaces are structurally anisotropic, with barbs and barbules arranged in a directional pattern, the orientation of the sessile drop relative to the barb axis can influence the measured contact angle. In this study, all droplets were placed on the dorsal surface of the pennaceous vane with the feather oriented tip-upward, maintaining a consistent measurement direction across all species and feather types. We did not measure directional CA (advancing, receding, or transverse), which means our static CA values capture a single orientation rather than the full anisotropic wetting behavior of the surface.

2.4. Computational Analysis and Statistical Methods

To model the relationship between feather microstructure and wettability, we assembled a dataset of 119 measurements across 12 species, where each set represents a mean of 25 points to minimize per-species error. The seven structural parameters (L_{basal}, L_{total}, R_{basal}, θ_{distal}, $\theta_{proximal}$, $\Delta\theta$, and $d_{barbule}$) were matched to a corresponding static CA.

We computed Pearson correlations at two levels in order to identify which parameters relate to CA. We first calculated pooled correlations across all measurements, then correlations across the 12 species means. We used both because pooled correlations capture relationships at the level of individual feathers, while species-level correlations remove within-species scatter and expose the structure that differs between species.

To determine how much contact-angle variation was systematic rather than individual, we split the total variance using a one-way analysis of variance (ANOVA). We split the sum of squares into between-species and within-species components and computed this partition both overall and within each habitat, since the balance of these components determines how well any model can learn from the data.

We employed four regression models to model the joint and non-linear effects of all seven parameters. We used linear regression as an interpretable baseline and generalized additive models (GAMs) to capture smooth non-linear effects. Random Forest and XGBoost are used

to capture non-linear interactions. Random Forest served as the primary model, and we reported performance as both R^2 and root mean square error (RMSE) so that accuracy was expressed in explained variance and in physical degrees.

To evaluate predictive performance and generalization, we applied three cross-validation schemes. We used five-fold cross-validation for strata above 30 samples and leave-one-out for smaller strata. We then applied leave-one-species-out (LOSO) cross-validation, in which the model was trained on 11 species and tested on the extra twelfth, because standard cross-validation allows measurements from the same species to fall into both training and test folds and therefore cannot test whether a model generalizes to a species it has never seen.

To test where structure predicts wettability, we stratified the data by biologically defined groups, evaluating model performance separately by habitat, by feather type, and by their combinations.

We again used a one-way ANOVA with Tukey HSD post-hoc comparisons to test differences among species, as well as a two-way ANOVA to test the interaction between habitat and feather type. For specific contrasts, we employed paired and species-level t-tests. Together, these statistical tests can minimize the error from a smaller sample size during stratification analysis.

To confirm that the primary correlation was stable given only 12 species, we applied resampling methods. We generated 10000 bootstrap resamples to estimate confidence intervals and ran 10000 permutations to assess significance, and we applied the same permutation approach to test the length-threshold effect. All analyses were performed in R using the RandomForest, XGboost, mgcv, and boot packages downloaded from online.

3. Results and Analysis

3.1. Cross-Species Overview: Contact Angle Differs Significantly Across Species

CA measurements for all 12 species remained above the 90° hydrophobic threshold and varied significantly, ranging from 94° to 133°, with 95% of the measurements falling between 95° and 129° (**Fig. 4A**). This variability is further supported by one-way Analysis of Variance (ANOVA, $p = 2.53\times10^{-6}$) and Tukey's Honestly Significant Difference (HSD), with 11 of 66 species pairs significant. Notably, Tukey pairs concentrate on extreme rather than mid-cluster measurements, indicating feathers concentrated at around 120° cannot be separated. The highest average CAs were observed from the Alexandrine parrot (123.9°), great white pelican (123.6°), and the Eurasian eagle owl (121.7°). The common ostrich exhibited the lowest

species-level mean CA (108.3°), while the lowest individual feather measurement was recorded for the ring-necked pheasant (94.3°).

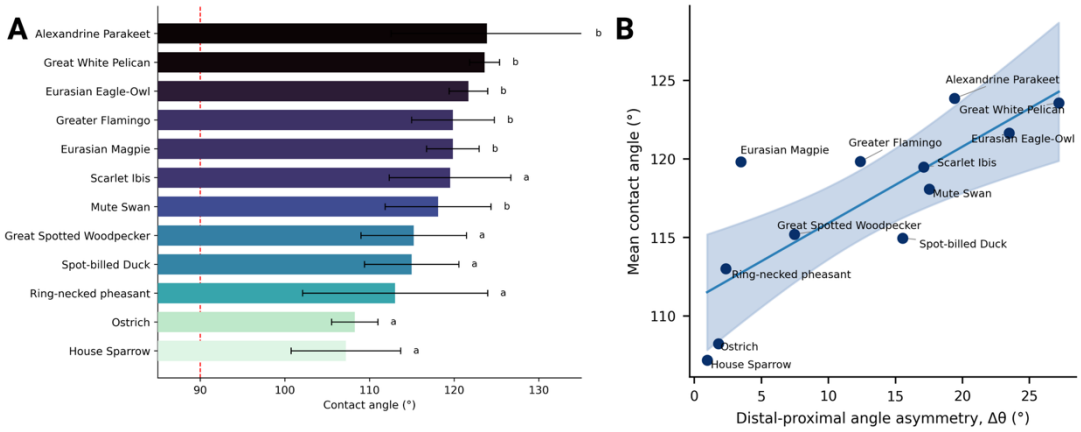


Figure 4. Key results of model predictions and validation of asymmetry across varying CA. (A) Static CA across the 12 sampled species. Bars show the mean CA with 95 percent confidence intervals. Species sharing a letter do not differ significantly (Tukey honestly significant difference test, $\alpha = 0.05$). CA differs significantly among species (one-way ANOVA, $p = 2.5 \times 10^{-6}$). The dashed line marks the 90 degree hydrophobicity threshold. (B) Distal-to-proximal barbule angle asymmetry as the dominant structural correlate of CA. Each point is a species mean. CA increases with angle asymmetry ($\Delta\theta$) at the species level ($r = 0.80$, 95 percent bootstrap confidence interval [0.48, 0.96], permutation $p = 0.002$).

3.2. Mechanistic Drivers in Pooled and Cross-Species Data: Asymmetry Influences Hydrophobicity

To understand the structural features driving the observed CA difference, we conducted Pearson correlation and across all 8 parameters first at the pooled level, where we considered each data point against all 119 feather measurements. Differences among the distal and proximal angles, or $\Delta\theta$, and the proximal angle, or θ_{proximal} , emerged as stronger drivers ($r = 0.332$, $r = -0.351$, respectively), compared to barbule spacing, or d_{barbule}, which exhibited a smaller r of -0.267. Since both $\Delta\theta$ and θ_{proximal} are collinear, we consider angle composition one of the crucial determinants of CA across habitat and evolutionary ranges. However, when comparing $\Delta\theta$ with its apparent contributing angles, it did not outperform the two raw angles jointly at the pooled level ($r = 0.263$ vs 0.467), suggesting pooled-level correlations may involve more complications than within-species level correlations, which focus on how each of the 12 species selected.

Interestingly, Δθ served as the only significant dominant structural correlate of CA at between-species level, with r = 0.800 and a bootstrap 95% CI ([0.49, 0.96]) (**Fig. 4B**). Significance was guaranteed on both tests (p = 0.0018, p = 0.0019, respectively). Barbule spacing, a parameter we expected to be a significant driver of CA, actually emerged as insignificant (p = 0.310) when investigating within-species-level predictors. To test whether the correlation translates into a meaningful group difference, we ranked species by their mean Δθ and split them into tertiles (four species each). A two-sample t-test on species-level mean CAs between the top and bottom tertiles yielded a significant difference (top tertile mean = 121.8°, bottom tertile mean = 112.1°, difference = 9.7°, t = 3.07, p = 0.022, Cohen's d = 2.17). When tested using all individual feather measurements pooled within each tertile group (n = 41 per group), the difference remained significant (t = 4.50, p < 0.001), though this feather-level test involves pseudoreplication. The species-level result is the conservative and appropriate test given our sampling design.

3.3. Computational Modeling: Structure Predicts Hydrophobicity in Non-Linear Models

Because feathers vary along seven correlated structural axes simultaneously and cannot be manipulated one at a time, we turned to Random Forest, XGBoost, and GAM models to evaluate all predictors jointly. Nonlinear models consistently outperformed linear models (R^2 = 0.130), with Random Forest depicting the highest R^2 of 0.509 (RMSE = 5.84°), winning 8 of 12 strata with 119 feather measurements (**Table 2**). XGBoost performed similarly with R^2 = 0.468, while GAM yielded a low R^2 of 0.066. Higher R^2 from non-linear models implies that the structural predictors interact rather than adding independently.

Table 2. Cross-validated R^2 and RMSE by stratum and model

Stratum	N *25	CV	Linear	GAM	RF	XGBoost
Full dataset	119 *25	5CV	0.130	0.066	**0.509**	0.468
Contour only	53 *25	5CV	0.377	0.363	**0.606**	0.578
Flight only	66 *25	5CV	-0.053	-0.579	**0.139**	-0.064
Aquatic all	49 *25	5CV	-0.007	-0.190	**0.253**	0.122
Terrestrial all	70 *25	5CV	0.160	0.233	**0.493**	0.379
Terrestrial + Contour	28 *25	LOO	0.547	**0.888**	0.833	0.797

Cross-validated R^2 for each regression model across strata. 5CV, five-fold cross-validation; LOO, leave-one-out; RF, Random Forest. Bold indicates the best-performing model within each stratum. Sample size (n) and cross-validation scheme are listed per stratum, where each data point represents a mean of 25, imputed into the model. Full-dataset RMSE was 5.84° and improved to 4.75° when restricted to larger feathers, both under Random Forest.

3.4. Stratification Analysis: Structure Predicts Best in Terrestrial Contour Feathers

We next assessed how ecological distinctions, such as habitat, feather size, and feather type, can influence wettability by stratifying biologically meaningful groups (**Fig. 5**).

Across all species, contour feathers produced an R^2 value of 0.606 (n = 53), while flight feathers only displayed an R^2 of 0.164 (n = 66), indicating flight feathers are unpredictable from geometry. Stratifying by aquatic compared to terrestrial birds yielded R^2 values of 0.253 and 0.493, respectively, validating habitat's influence on the predictability of structures.

Notably, in terrestrial contour feathers, Random Forest reached an R^2 value of 0.833, which represents a significant difference compared to aquatic contour feathers with an R^2 of 0.137. This stark discrepancy suggests that while terrestrial contour feather functionality is tightly coupled to overall geometry, aquatic contour feathers may be subject to evolutionary pressures. However, the small sample size of less than 30 measurements may limit this interpretability.

To determine the potential cause for this discrepancy and variance decomposition, we tested one-way ANOVA and determined that aquatic species retained only 11.9% between-species variation, while within-species variation reached 88.1%. Such low variance

corresponds to its low R^2 value, since there is little systematic variation for models to learn. On the other hand, terrestrial species exhibited 41.1% between-species variation but only 58.9% within-species variation. Observational bootstrap confirmed non-overlapping 95% confidence intervals (aquatic [6.8%, 28.8%], terrestrial [34.8%, 60.1]).

A two-way ANOVA revealed a significant interaction between habitat and feather type ($p = 0.034$), indicating that the effect of feather type on CA depends on the bird's habitat. This interaction was driven by aquatic species. Among aquatic birds, contour feathers reached the highest mean CA of any group at 122.5 degrees, exceeding that of aquatic flight feathers. This aquatic contour advantage was consistent in direction but fell just short of statistical significance in the specific pairwise comparison (paired $p = 0.0501$, species-level $p = 0.062$), so we report it as a trend rather than a confirmed difference. Terrestrial birds showed no such pattern. Contour and flight feathers did not differ in terrestrial species ($p = 0.692$), which indicates that feather-type specialization for water repellency is specific to aquatic birds rather than a general feature across habitats.

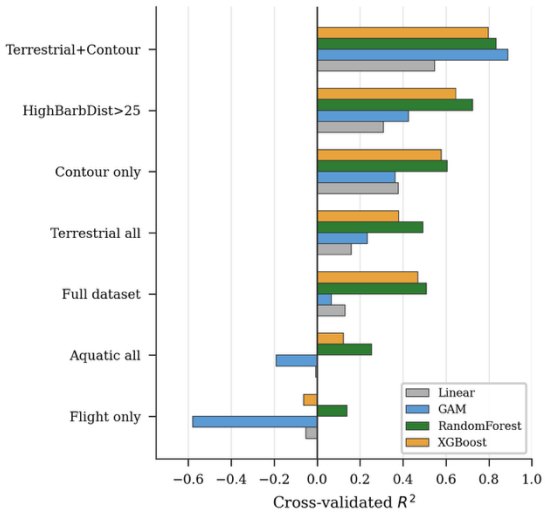


Figure 5. Cross-validated coefficient of determination (R^2) for four regression models across feather strata, ordered from highest to lowest predictive performance. Values are five-fold cross-validated for strata above 30 samples and leave-one-out for smaller strata.

When investigating how barbule length contributes to model responses, prediction accuracy was somewhat higher among structurally larger feathers, with more regular microstructures, though this effect was modest and partly reflected the exclusion of small-feathered terrestrial species.

Taken together, model performance and structural changes vary between terrestrial and aquatic species as well as flight and contour feathers. Flight feathers are much harder to predict

efficiently compared to contour feathers, where terrestrial species demonstrate more compatibility with models. Aquatic and terrestrial birds show different species variations, which could be driven by how habitat interacts with microstructure.

To quantify the relative contribution of each parameter, we extracted permutation importance and SHAP (SHapley Additive exPlanations) values from the full-dataset Random Forest (**Fig. 6**). Δθ ranked first by permutation importance ($\Delta R^2 = 0.204$), followed by $\theta_{proximal}$ (0.189) and θ_{distal} (0.124). SHAP values confirmed this ranking, where $\theta_{proximal}$ and Δθ each shifted predictions by approximately 1.4 to 1.5° on average, while $d_{barbule}$ contributed 0.79°. The three length parameters (L_{basal}, L_{total}, R_{basal}) collectively accounted for roughly one-third of the model's predictive capacity, consistent with their roles as nonlinear modulators rather than dominant linear drivers. Interestingly, in the terrestrial contour stratum, θ_{distal} became the top-ranked feature by SHAP (1.55°), overtaking Δθ (1.45°), which suggests that for feathers where geometry predicts CA most accurately, the absolute distal angle carries additional information beyond what the asymmetry index captures alone.

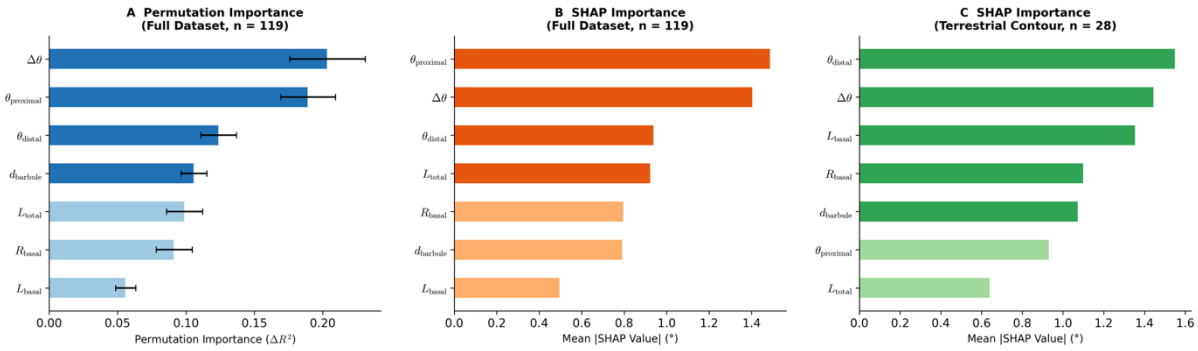


Figure 6. Relative importance of seven barbule parameters in predicting contact angle under Random Forest. (A) Permutation importance (ΔR^2) for the full dataset (n = 119). Error bars show standard deviation across 20 permutation repeats. (B) Mean absolute SHAP values for the full dataset. (C) Mean absolute SHAP values for the terrestrial contour stratum (n = 28). Darker bars highlight features exceeding the threshold of $\Delta R^2 > 0.10$ in (A) and mean |SHAP| > 0.9° in (B) and > 1.0° in (C).

3.5. Generalization and Variance Structure: Models Cannot Extrapolate Across Species

We next questioned whether utilizing the strength of within-group models mentioned can capture generalizable structure for species outside of trained datasets. Under Leave-One-Species-Out (LOSO) cross-validation, every model collapses to R^2 less than 0 (Linear −0.079, GAM −3.403, Random Forest −0.096, XGBoost −0.459), suggesting models fail to predict new species' CA performance (**Fig. 7**). When investigating causes for this collapse, one-way ANOVA results expose how between-species analysis explains only 34.2% of the total CA

variance, while within-species explains 65.8% of total CA variance. With little systematic between-species signal and only 12 species, cross-species extrapolation becomes difficult, extending to low r values in pooled coefficients. Therefore, model results are within-taxa structural optimization tools and cannot be used as phenotype predictors for new species.

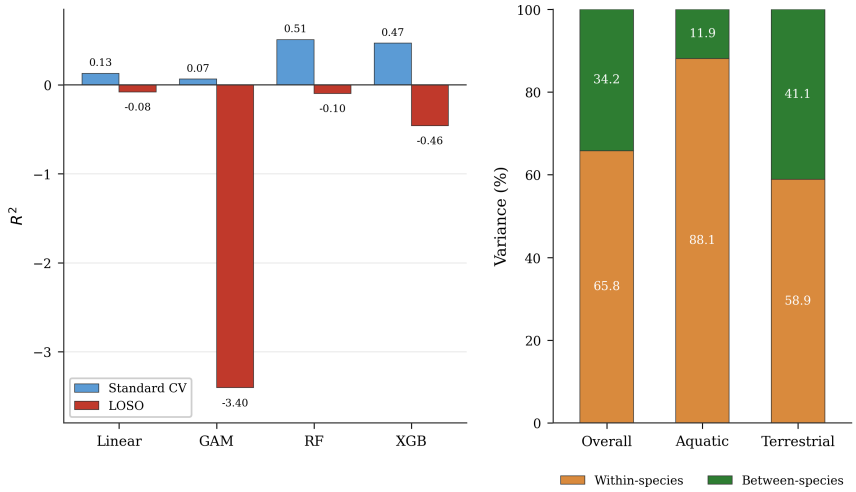


Figure 7. Model generalization and variance structure that constrains it. (Left) Coefficient of determination (R^2) under standard cross-validation compared with leave-one-species-out (LOSO) cross-validation, in which models trained on 11 species predict the held-out twelfth. All models collapse below zero under LOSO, showing that CA cannot be predicted for a species absent from training. (Right) Partition of total contact-angle variance into within-species and between-species components, computed overall and within each habitat.

3.6. Verification Through 3D Fabrication of Feather Microstructures Confirms Model Robustness

The stratified models identify how much of wettability structure explains, but designing a physical surface requires knowing the direction each parameter should move. We therefore extracted the direction of effect for each predictor from the models. CA was predicted to rise with greater $\Delta\theta$ and with a higher basal lamella fraction, and to fall with wider barbule spacing and $\theta_{proximal}$. We then fabricated three geometries to test their resulting CA. A high-performance design maximized the strongest predictors, a low-performance design minimized them, and a third design replicated the Alexandrine Parakeet contour feather as a biological reference (**Fig. 8A-G**).

The measured CA followed the model's strongest prediction closely. The three designs ranked precisely by angle asymmetry in terms of CA measurements, with the high-performance

design at 90.704°, the biological reference at 84.998°, and the low-performance design at 62.301° (**Fig. 8H-K**), matching their asymmetry values (15°, 10°, and 0°, respectively). The high-performance design also carried the highest basal lamella fraction at 0.80.

However, two parameters did not follow their individual predictions. The high-performance design had wider barbule spacing than the parrot reference(28 µm to 19µm), and a larger $\theta_{proximal}$ (33° to 18°), both of which would predict a lower CA in isolation. Since we do not know which parameter contributed more to the final CA value, it remains hard to ascertain whether each change improved or decreased individual CA measurements, but the high CA achieved by the high-performance group confirms that wettability is governed by the combination of parameters rather than any single one, which is the reason a multivariable model was necessary.

Together, printed validations confirm that structure alone, without favorable surface chemistry, can convert a hydrophilic material toward hydrophobicity, especially with asymmetry-driven design that outperformed biological controls.

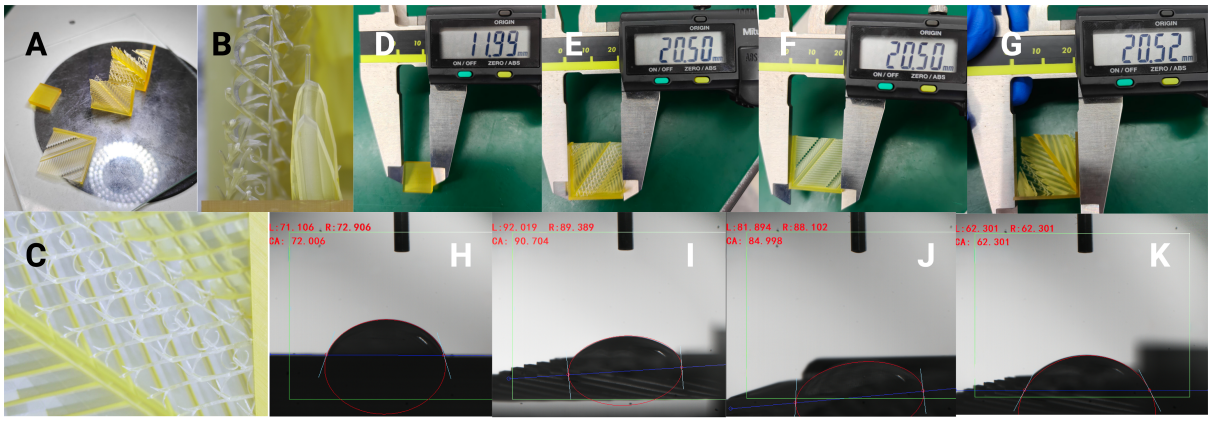


Figure 8. Biomimetic validation of asymmetry predictor. (A) The four experimental groups shown together, printed by stereolithography and scaled 20x of the original due to printing constraints. (B) Printed microstructures demonstrating layered effects of low-performance geometry. (C) Printed microstructures demonstrating layered effects of high-performance geometry. (D) Flat HTL resin control. (E) Model-optimized high-performance geometry. (F) Biological reference replicating the Alexandrine parakeet. (G) Model-predicted low-performance geometry. (H-K) Static contact-angle measurements. Structures ranked in CA by their angle asymmetry, with the high-performance design at 90.7° (I), the biological reference at 85.0° (J), and the low-performance design at 62.3° (K), against a flat control of 72.0° (H). Geometry alone raised the CA above the 90° hydrophobic threshold on an intrinsically hydrophilic HTL resin.

4. Discussion

This work quantified barbule-level microgeometry across 12 species of birds spanning avian phylogeny and habitats in relation to static CA. We used multivariable machine learning to identify which structural parameters governed hydrophobicity, then validated the strongest predictors by fabricating and testing 3D-printed geometries, yielding a 25.97% increase in CA through structure alone. Insights into microgeometry optimization remain crucial in designing passive and sustainable hydrophobic structural surfaces, in contrast to many existing chemical alternatives that actively degrade and contaminate the environment. Variation among habitats and strategies to achieve hydrophobicity from birds also carry a unique value compared with existing biomimetic approaches such as the lotus leaf: their natural adaptations can be customized to serve optimized purposes under varying aquatic or terrestrial settings for environmental engineers.

4.1. Mechanistic Explanations and Habitat-Dependent Strategies

We identified distal-proximal angle asymmetry, or $\Delta\theta$, as the dominant structural predictor for high hydrophobicity, a parameter currently unrecorded and unquantified in existing literature. A mismatch between distal and proximal barbule angles produces an anisotropic, multi-directional mesh, which plausibly stabilizes the trapped air layer of the Cassie–Baxter state more effectively than a symmetric arrangement. Further, asymmetric barbule angles create non-uniform pore geometries that resist the capillary pressure needed for Wenzel transition, as demonstrated by a 7° improvement in highly asymmetric feathers within our dataset. However, $\Delta\theta$ alone (single-feature $R^2 = 0.26$) does not out-predict the two raw angles jointly ($R^2 = 0.47$), so its value is for species-level interpretations rather than for new species.

One feasible explanation for high CA among contour feathers but not flight feathers is that flight feathers are optimized for aerodynamic and mechanical performance, so their wettability is less tightly coupled to barbule geometry. This can represent a functional trade-off for birds to maneuver in the air and develop varying structures in different body parts. Since geometry predicts CA strongly in terrestrial contour feathers ($R^2 = 0.83$) but weakly in aquatic contour feathers ($R^2 = 0.14$), aquatic species may converge on similar microstructures, resulting in little signal for models to develop predictions. This is consistent with only 11.9% between-species variance (compared to 41.1% in terrestrial species). For this very reason, models cannot extrapolate to a phylogenetically novel species, considering 66% of CA variance lies within species. Therefore, model results greatly depend on data size and species selection.

We observed a significant habitat-to-feather-type interaction (two-way ANOVA, $p = 0.034$), indicating the effect of feather type on wettability depends on habitat. The high mean CA of 122.5° observed in aquatic contour feathers is consistent with the constant need for body feathers to shed water and maintain buoyancy in aquatic species. This difference was mirrored between aquatic flight and contour feathers, but interestingly not within terrestrial birds ($p = 0.692$). Hence, feather-type specialization for CA seems to be specific to aquatic birds.

The three length-related parameters contributed modestly. L_{basal} showed no significant pooled correlation with CA ($r = 0.156$, $p = 0.091$), L_{total} was weakly negative ($r = -0.180$, $p = 0.050$), and R_{basal} was nonsignificant ($r = 0.141$, $p = 0.126$). None reached significance at the species level (all $p > 0.45$). However, Random Forest feature importance revealed that L_{total} and R_{basal} ranked third and fourth by permutation importance ($\Delta R^2 = 0.099$ and 0.092, respectively), indicating they contribute to CA prediction through nonlinear interactions that Pearson correlations cannot capture.

4.2. Interpretation of Fabrication Results

3D fabrication represents the final step of this study's closed-loop framework, where it verifies the model's within-range recommendations physically. The model-optimized design exceeded the flat control by 18.7°, and the biological parrot reference by 5.7°, showing that an engineered geometry can match or exceed a naturally evolved one. However, not all parameters are closely aligned. With wider barbule spacing and a larger proximal angle, both models contradict their corresponding predictions but still support a high CA measurement. Together, these variations indicate wettability can be influenced by a combination of parameters rather than a single one, reinforcing the necessity of multivariable models. One reason for borderline hydrophobic values compared to actual feather CA measurements may be the composition of materials. Since HTL resin is inherently hydrophilic, its measurement cannot rival the keratin of natural feathers but is able to depict the full effect of structure-level changes.

One important caveat is that all fabricated structures were scaled to 20 times the natural barbule dimensions due to the resolution limits of the stereolithography printer. At natural scales, barbule features measure roughly 10 to 30 μm, placing them well below the capillary length of water (approximately 2.7 mm), where the Cassie-Baxter air-trapping mechanism operates most effectively. Despite this limitation, the consistent ranking of CA across all three printed geometries, and the fact that asymmetry still governed performance in the same

direction predicted by the biological data, suggests that the relative contribution of each geometric parameter is preserved even at enlarged scale.

4.3. Limitations

Numerous limitations exist in the phylogenetic, sampling, and modeling of this study (**Fig. 8**). First, with only 12 species and several aquatic species drawn from the same order, apparent convergence in hydrophobic performance cannot be distinguished from shared ancestry. Since no correction was applied, models may report species similarity in microstructures as a result of a pattern in CA rather than underlying evolutionary mechanisms. Second, multiple feathers and data points taken within a single species violate the independence assumption of ordinary regression. However, we mitigated this effect by analyzing at the species level for key claims, but a mixed-effects framework would be the statistically ideal treatment. Thirdly, leave-one-species-out cross-validation failure indicates that models applied in the analysis portions are restricted to biological datasets and cannot predict new species. Therefore, tree models such as Random Forest cannot extrapolate above the training maximum of (133°). Lastly, one of the main caveats is the small sample size of n=28 for stratification analysis. As a result, R2 values should be interpreted as promising but sample-limited. Despite this, 3D fabrication did demonstrate robustness of some predictions with its CA increase.

4.4. Implications

From the methodological standpoint, we establish that single structural indices, such as barbule spacing alone, are insufficient to predict hydrophobicity, and the factors guiding its mechanism can be mapped with non-linear computational modeling.

From a biological perspective, we identified a previously undocumented structural predictor for hydrophobicity. Additionally, between/within species results demonstrate clear differences among habitat and feather types, with aquatic species correlating with more conserved structures while terrestrial species correlating with more variance.

From an engineering lens, because structure alone shifted a hydrophilic material across the hydrophobic threshold, feather-inspired asymmetric structures offer a route to chemistry-free water repellency, which is relevant to sustainable coatings that avoid persistent fluorinated compounds.

4.5. Applications

Because structure alone raises the contact angle across the hydrophobic threshold on hydrophilic resin, our work may address the central limitation of conventional hydrophobic surfaces, which rely on fluorinated or silicone treatments that degrade and persist as environmental contaminants. Therefore, fields involving self-cleaning surfaces for infrastructure, moisture-resistant materials, and aerospace or wind-energy anti-icing may consider an alternative where the flexible (if geometry uses flexible materials) and resilient nature of feather-derived architecture can be used over rigid surfaces (**Fig. 9**). Additionally, our biology-to-model-to-fabrication pipeline, as well as data extraction, can be applied to engineering and bioinformatics. However, since current structures remain under restrictions and are not printed on materials that enable the superhydrophobic regime, its immediate applications should serve as enhancements rather than replacements for high-performance coatings.

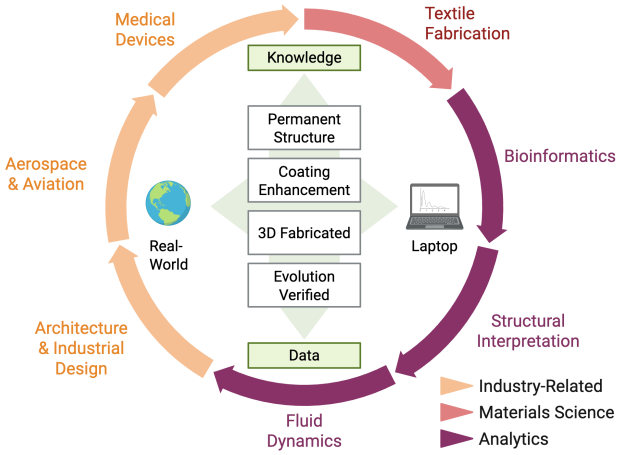


Figure 9. Potential application domains for structurally driven, chemistry-free water repellency derived from the asymmetry design principle, including water-repellent structures, self-cleaning surfaces, textiles, and aerospace. Computational methods may be applied to bioinformatics. Created with BioRender.

4.6. Future Work

While this research achieves strong preliminary results, it also serves as proof of the intricacies of feather microstructures, inviting more investigation into how predicted trends can be modeled into engineered solutions.

To separate convergence from shared ancestry, using phylogenetic generalized least squares (PGLS) to apply corrections to existing predictions can control species non-independence [16], [25]. Although fabricated models already validate model-predicted claims,

expanding species sampling can help solidify generalizable trends. Current 3D-printed prototypes can also be printed with higher-precision printers and a scale closer to a feather's natural microstructures, using materials similar to natural keratin [26]. Added nanotopography on top of existing microstructures can mimic the combined hydrophobic performance on engineered surfaces [27], [28]. Lastly, to investigate the interactions with surface and keratin-based chemistry, Fourier transform infrared (FTIR) spectroscopy can be applied to separate contributions of the rachis keratin with its structures [26].

5. Conclusion

In conclusion, this study demonstrates that avian feather microstructure provides a robust, chemistry-free structural mechanism for hydrophobicity, with distal–proximal barbule angle asymmetry ($\Delta\theta$) emerging as the dominant species-level predictor rather than any single absolute dimension such as barbule spacing or total length. Across 12 species, feather surfaces remained hydrophobic (CA 94-133°), and species-level $\Delta\theta$ correlated strongly with CA ($r=0.80$; 95% bootstrap CI [0.485,0.956]; permutation $p \approx 0.002$), with high-asymmetry feathers averaging 121.8° versus 113° for low-asymmetry feathers. Multivariable models showed that hydrophobicity is governed by nonlinear interactions among structural parameters: Random Forest reached cross-validated $R^2=0.509$ for the full dataset and $R^2=0.833$ for terrestrial contour feathers, but performance collapsed under leave-one-species-out validation, and within-species variation dominated overall variance (65.8%, rising to 88.1% in aquatic birds), indicating that current models are powerful within biological groups but not yet generalizable across species. The asymmetry principle was physically validated through stereolithography: high-, biological-reference-, and low-asymmetry designs ranked exactly by CA at 90.7°, 85.0° and 62.3°, respectively, versus 72.0° for a flat control; the high-performance design increased CA by 18.7° (25.97%) and crossed the 90° hydrophobic threshold on an intrinsically hydrophilic resin, confirming that geometry alone can rival chemical treatment. These findings establish a closed-loop biology-to-model-to-fabrication framework for sustainable water-repellent surfaces, while also highlighting limitations in species sampling, phylogenetic independence, and small stratified sample sizes; future work should incorporate phylogenetic comparative methods, mixed-effects models, broader species coverage, higher-precision keratin-like fabrication, and multi-scale hierarchical texture to move from hydrophobic toward superhydrophobic performance.

References

[1] M. J. Wood, G. Brock, and A.-M. Kietzig, "The penguin feather as inspiration for anti-icing surfaces," *Cold Regions Science and Technology*, vol. 213, p. 103903, Sep. 2023, doi: 10.1016/j.coldregions.2023.103903.

[2] G. Liu *et al.*, "A review of various self-cleaning surfaces, durability and functional applications on building exteriors," *Construction and Building Materials*, vol. 409, p. 134084, Dec. 2023, doi: 10.1016/j.conbuildmat.2023.134084.

[3] K. Taliantzis and K. Ellinas, "Green hydrophobic and superhydrophobic coatings and surfaces for water related applications: A review," *Advances in Colloid and Interface Science*, vol. 343, p. 103566, Sep. 2025, doi: 10.1016/j.cis.2025.103566.

[4] C. Costa, C. Silva, E. F. Marques, and N. G. Azoia, "A sustainable approach for providing water repellency in textiles by using long-chain cellulose esters," *Cellulose*, vol. 30, no. 11, pp. 7347–7362, Jul. 2023, doi: 10.1007/s10570-023-05311-8.

[5] J. N. Meegoda, J. A. Kewalramani, B. Li, and R. W. Marsh, "A Review of the Applications, Environmental Release, and Remediation Technologies of Per- and Polyfluoroalkyl Substances," *International Journal of Environmental Research and Public Health*, vol. 17, no. 21, p. 8117, Jan. 2020, doi: 10.3390/ijerph17218117.

[6] H. Zhang *et al.*, "Progress of fluorine-free water repellents for textiles: A comprehensive review from industry and academia," *Progress in Organic Coatings*, vol. 213, p. 109948, Apr. 2026, doi: 10.1016/j.porgcoat.2026.109948.

[7] A. L. Ling, "Estimated scale of costs to remove PFAS from the environment at current emission rates," *Science of The Total Environment*, vol. 918, p. 170647, Mar. 2024, doi: 10.1016/j.scitotenv.2024.170647.

[8] H. J. Ensikat, P. Ditsche-Kuru, C. Neinhuis, and W. Barthlott, "Superhydrophobicity in perfection: the outstanding properties of the lotus leaf," *Beilstein J. Nanotechnol.*, vol. 2, no. 1, pp. 152–161, Mar. 2011, doi: 10.3762/bjnano.2.19.

[9] M. Sun, G. S. Watson, Y. Zheng, J. A. Watson, and A. Liang, "Wetting properties on nanostructured surfaces of cicada wings," *J Exp Biol*, vol. 212, no. 19, pp. 3148–3155, Oct. 2009, doi: 10.1242/jeb.033373.

[10] A. B. D. Cassie and S. Baxter, "Wettability of porous surfaces," *Trans. Faraday Soc.*, vol. 40, pp. 546–551, Jan. 1944, doi: 10.1039/TF9444000546.

[11] E. Bormashenko, Y. Bormashenko, T. Stein, G. Whyman, and E. Bormashenko, "Why do pigeon feathers repel water? Hydrophobicity of pennae, Cassie–Baxter wetting hypothesis and Cassie–Wenzel capillarity-induced wetting transition," *Journal of Colloid and Interface Science*, vol. 311, no. 1, pp. 212–216, Jul. 2007, doi: 10.1016/j.jcis.2007.02.049.

[12] F. M. S. Muzio and M. A. Rubega, "What do we really know about the water repellency of feathers?," *Journal of Avian Biology*, vol. 2024, no. 11–12, p. e03259, 2024, doi: 10.1111/jav.03259.

[13] A. M. Rijke, "The Water Repellency and Feather Structure of Cormorants, Phalacrocoracidae," *J Exp Biol*, vol. 48, no. 1, pp. 185–189, Feb. 1968, doi: 10.1242/jeb.48.1.185.

[14] A. M. Elowson, "Spread-Wing Postures and the Water Repellency of Feathers: A Test of Rijke's Hypothesis," *Auk*, vol. 101, no. 2, pp. 371–383, Apr. 1984, doi: 10.1093/auk/101.2.371.

[15] S. Srinivasan *et al.*, "Quantification of feather structure, wettability and resistance to liquid penetration," *J. R. Soc. Interface.*, vol. 11, no. 96, p. 20140287, Jul. 2014, doi: 10.1098/rsif.2014.0287.

[16] P. L. Pap *et al.*, “A phylogenetic comparative analysis reveals correlations between body feather structure and habitat,” *Functional Ecology*, vol. 31, no. 6, pp. 1241–1251, 2017, doi: 10.1111/1365-2435.12820.
[17] P. L. Pap *et al.*, “Interspecific variation in the structural properties of flight feathers in birds indicates adaptation to flight requirements and habitat,” *Functional Ecology*, vol. 29, no. 6, pp. 746–757, 2015, doi: 10.1111/1365-2435.12419.
[18] F. M. S. Muzio, M. Çam, A. Tarakanova, and M. A. Rubega, “Exploring the role of barbule density in feather water repellency: insights from 3D modeling and a comparative analysis,” *J Exp Biol*, vol. 229, no. 17, p. jeb252368, Sep. 2026, doi: 10.1242/jeb.252368.
[19] H. D. Branion, “Avian Anatomy–Integument,” *Poultry Science*, vol. 53, pp. 447–448, Jan. 1974, doi: 10.3382/ps.0530447a.
[20] D. W. Snow, “Skin and feather,” *Nature*, vol. 248, no. 5449, pp. 620–620, Apr. 1974, doi: 10.1038/248620a0.
[21] A. Azimi Yancheshme, S. Hassantabar, K. Maghsoudi, S. Keshavarzi, R. Jafari, and G. Momen, “Integration of experimental analysis and machine learning to predict drop behavior on superhydrophobic surfaces,” *Chemical Engineering Journal*, vol. 417, p. 127898, Aug. 2021, doi: 10.1016/j.cej.2020.127898.
[22] Y.-J. Chen *et al.*, “White Roman Goose Feather-Inspired Unidirectionally Inclined Conical Structure Arrays for Switchable Anisotropic Self-Cleaning,” *ACS Appl Mater Interfaces*, vol. 16, no. 28, pp. 36840–36850, Jul. 2024, doi: 10.1021/acsami.4c09082.
[23] S. Valladares, R. Moreno, L. Jover, and C. Sanpera, “Evaluating cleansing effects on trace elements and stable isotope values in feathers of oiled birds,” *Ecotoxicology*, vol. 19, no. 1, pp. 223–227, Jan. 2010, doi: 10.1007/s10646-009-0407-1.
[24] T. Young, “III. An essay on the cohesion of fluids,” *Phil. Trans. R. Soc.*, no. 95, pp. 65–87, Dec. 1805, doi: 10.1098/rstl.1805.0005.
[25] C. K. Cornwallis and A. S. Griffin, “A Guided Tour of Phylogenetic Comparative Methods for Studying Trait Evolution,” *Annual Review of Ecology, Evolution, and Systematics*, vol. 55, pp. 181–204, 2024, doi: 10.1146/annurev-ecolsys-102221-050754.
[26] L. R. Treviño-Cervantes, A. Colín-Cruz, A. L. Martínez-Hernández, V. Saucedo-Rivalcoba, P. E. García-Casillas, and C. Velasco-Santos, “Surface modification of keratin from agro-industrial products treated by green processes to generate sustainable materials,” *Sustainable Chemistry and Pharmacy*, vol. 44, p. 101959, Apr. 2025, doi: 10.1016/j.scp.2025.101959.
[27] “What do we really know about the water repellency of feathers? - Muzio - 2024 - Journal of Avian Biology - Wiley Online Library.” Accessed: Sep. 13, 2026. [Online]. Available: https://nsojournals.onlinelibrary.wiley.com/doi/10.1111/jav.03259
[28] M. Mao, J. Wei, B. Li, L. Li, X. Huang, and J. Zhang, “Scalable robust photothermal superhydrophobic coatings for efficient anti-icing and de-icing in simulated/real environments,” *Nature Communications*, vol. 15, no. 1, pp. 1–12, Nov. 2024, doi: 10.1038/s41467-024-54058-8.